The Charge Density Distribution in a Model Compound of the Catalytic Triad in Serine Proteases

Jacob Overgaard, Birgit Schiøtt, Finn K. Larsen, and Bo B. Iversen*[a]

Abstract: Combined low temperature (28(1) K) X-ray and neutron diffraction measurements were carried out on the co-crystallised complex of betaine, imidazole, and picric acid (**1**). The experimental charge density was determined and compared with ab initio theoretical calculations at the B3LYP/6–311G(d,p) level of theory. The complex serves as a model for the active site in, for example, the serine protease class of enzymes, the so-called catalytic triad. The crystal contains three short strong N–H···O hydrogen bonds (HBs) with $d_{N\cdots O} < 2.7$ Å. The three HBs have energies above 13 kcal mol^{-1}, although the hydrogen atoms are firmly localized in the "nitrogen wells". This suggests that low-barrier hydrogen bonding in catalytic enzyme reactions may be a sufficient, but not a necessary, condition for obtaining transition-state stabilization. Structural analysis (e.g., covalent N–H bond lengthening) indicates that the hydrogen bond between H3A and O8 of imidazole and betaine respectively (HB2) is slightly stronger than the bond between H1A and O1A of imidazole and picric acid (HB1), although HB1 is shorter than HB2: ($d_{N\cdots O}$(HB1) = 2.614(1) Å, $d_{N\cdots O}$(HB2) = 2.684(1) Å, $d_{H\cdots O}$(HB1) = 1.630(1) Å, $d_{H\cdots O}$(HB2) = 1.635(1) Å, d_{N-H}(HB1) = 1.046(1) Å, d_{N-H}(HB2) = 1.057(1) Å). Furthermore, the charge density analysis reveals that HB2 has a larger covalent character than HB1, with considerable polarization of the density towards the acceptor atom. The Gatti and Bader source function (*S*) is introduced to the analysis of strong HBs. The source function is found to be a sensitive measure for the nature of a hydrogen bond, and comparison with low-barrier and single-well hydrogen bonding systems (e.g., benzoylacetone and nitromalonamide) shows that the low-barrier hydrogen bond (LBHB) state is characterized by an enormously increased hydrogen atom source contribution to the bond critical point in the HB. In this context, HB2 can be characterized as intermediate between localized HBs and delocalized LBHBs.

Keywords: charge density analysis · density functional calculations · enzyme catalysis · hydrogen bonds

Introduction

During the last decade, there has been intense debate about the origin of the rate-enhancing effect observed upon the involvement of enzymes in different chemical reactions. One of the most studied classes of enzymes is serine proteases, which are characterized by the presence of the catalytic triad, a specific spatial arrangement of three amino acid residues in the active site (Figure 1).[1] A number of researchers have proposed that one very strong, short hydrogen bond (HB) between a histidine and an aspartate residue, also known as a low-barrier hydrogen bond (LBHB), could be the major reason for the free-energy reduction necessary to increase the rate constant. Thus, the LBHB is postulated to be present in the transition state (TS) in the formation of the tetrahedral intermediate.[2] The excess bonding energy of an LBHB in comparison to an ordinary, weak HB easily amounts to 5–10 kcal mol^{-1}.[3] Warshel and co-workers oppose the LBHB

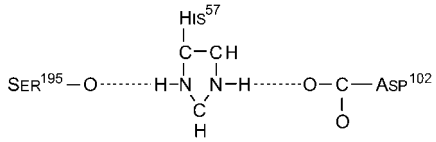

Figure 1. Schematic drawing of the catalytic triad. No formal charges or bonds orders are assumed in the sketch.

[a] Associate Professor B. B. Iversen, J. Overgaard, Dr B. Schiøtt, Associate Professor F. K. Larsen
Department of Chemistry
University of Aarhus
8000 Aarhus C (Denmark)
Fax: (+45) 86-196-199
E-mail: bo@chem.au.dk

Supporting information for this article is available on the WWW under http://www.wiley-vch.de/home/chemistry/or from the author and includes: atomic positional and displacement parameters from the neutron diffraction study and cif-file and multipole parameters for the X-ray study of **1**; source function contributions to the density at the strong HBs in **1**, benzoylacetone, and nitromalonamide; and residual density plots in imidazole ring A, imidazole ring B, picric acid A, picric acid B, and in the carboxylate group of betaine.

  0947-6539/01/0717-3756 $ 17.50+.50/0

mechanism and argue that a LBHB will have an anticatalytic effect in enzymes due to the polarity of the active site cavity and the presence of water molecules.[4] However, it should be noted that these conclusions are based on speculations about the charge distribution in LBHB systems.[5] The assumption that LBHB systems are largely uncharged has been challenged in recent studies of the LBHB of benzoylacetone.[6]

In a series of papers,[7] McAllister and co-workers study the effects of the surroundings on ideal LBHBs versus weak HBs by using high-level ab initio calculations on small model compounds. They find that deviations from idealized conditions (such as symmetrical solvation) have a large impact on LBHBs, but that LBHBs remain stronger than localized weak HBs, which are largely unaffected by changes in the surroundings. Other theoretical investigations focus on the effect of differences in proton affinities between the donor and the acceptor molecules on the formation of LBHBs.[8] It has been suggested that a prerequisite for LBHB formation is a ΔpK_a between donor and acceptor molecule of less than one unit. This criterion is limited by the absence of knowledge of proton affinities in environments such as enzymatic active sites or in crystalline materials. The issue of pK_a matching has been the center of much of the debate on the LBHB mechanism. In this respect, it has been demonstrated both theoretically[8c] and experimentally[9] that although HBs are strongest in pK_a matched systems, there is no special stabilization. In other words, linear relationships have been established between ΔpK_a and E_{HB} (hydrogen-bond energy). Some theoretical studies have proposed that E_{HB} follows a linear relationship with respect to the heteroatom separation ($d_{O\cdots O}$),[7e, 8c] while other studies find nonlinear relationships.[7a,c] It should be noted that $d_{O\cdots O}$ is only a relevant parameter in geometrically linear HBs. It is well established that HB strength depends on the bonding angle,[10] and, therefore, a more relevant parameter is $d_{H\cdots O}$. Espinosa and co-workers have studied 83 HBs with X-ray charge density and ab initio theoretical methods and found that exponential relations exist between E_{HB} and $d_{H\cdots O}$.[11] This suggests that HBs become *much* stronger when they are very short.

The complicated nature of short HBs can be exemplified by comparing the pK_a-matched systems of acetylacetone[12] and malonaldehyde[13] with the pK_a-mismatched system of benzoylacetone.[6] In these systems, the pK_a-matched systems have longer heteroatom separations (2.55 – 2.58 Å) than the mismatched systems (2.50 Å) at all levels of theory.[6b] This has been rationalized as being due to the presence of steric strain in benzoylacetone. Relief of the strain was found to be important for the formation of the LBHB state.[6c] Thus, although the general principles that govern HB interactions are well understood and many useful structural correlations have been established,[14] there are fine effects which can significantly alter a HB. The local environmental effects are especially important for short HBs, in which small factors may apparently change a delocalized HB (e.g., benzoylacetone[6]) to a localized HB (e.g., citrinin[15]) with almost equal $d_{O\cdots O}$.

We have studied the charge distributions of short HBs in crystals in order to improve the fundamental understanding of LBHBs.[6, 16] Such studies can provide information about the electronic structure and energetics of HBs and are relevant to discussions of LBHBs in enzyme catalysis. Only a few accurate electron density distribution (EDD) studies of LBHBs have appeared in the literature and they all concern O–H···O interactions.[6, 15, 16b–c, 17] Since the proposed LBHB in the catalytic triad is an N–H···O bond, we have extended these studies.[18] In this paper, we present a study of the charge distribution in the co-crystal of picric acid, imidazole, and betaine (**1**; Figure 2), which serves as a model compound for the catalytic triad. This study combines analysis of very low temperature X-ray (28 K) and neutron diffraction data (28 K), solid-state NMR data, and high-level density functional theory (DFT) calculations. The overall resemblance of **1** to the catalytic triad makes it one of the best model compounds for the serine protease catalytic triad, which has so far been studied by physicochemical methods. A preliminary account of the work has been published,[16a] in which topological methods were used to assess the strength of the three short N–H···O HBs. In this paper we present an analysis of the whole structure and directly compare experimental and high-level ab initio theoretical results. This comparison extends beyond the typical comparison of geometry and tests the adequacy of current theory to reproduce fine details of the EDD. We also introduce the source function by Gatti and Bader[19] into the analysis of HBs. The source function is found to be a sensitive measure of HB character.

Results and Discussion

Structural analysis: A complete list of the refined geometries of the three most important N–H···O interactions is given in Table 1, in which the following abbreviations for the HBs are introduced: HB1: N1A–H1A···O1A; HB2: N3A–H3A···O8; HB3: N1B–H1B···O1B. In HB1, the heteroatom separation ($d_{N\cdots O} = 2.614(1)$ Å) is smaller than the sum of the van der Waal's radii of the individual atoms (2.65 Å for N and O). In both HB2 (2.684(1) Å) and in HB3 (2.676(1) Å) the sum is larger. If the heteroatom distance criterion proposed by Hibbert and Elmsley[3] is used, all three N–H···O interactions qualify as strong HBs. Since this distance neglects the N–H···O angle, which is significantly different in each of the three HBs, it is more appropriate to consider $d_{H\cdots O}$. A comparison of the values of $d_{H\cdots O}$ shows that HB1 and HB2 are of similar strength (1.630(1) Å vs 1.635(1) Å) although HB3 is weaker (1.681(1) Å).

An extensive structural study has been carried out by Steiner which correlates the d_{N-H} and the $d_{H\cdots O}$ bond lengths in N–H···O HBs.[14] Based on neutron diffraction studies of N–H···O HBs and discrimination between two- and three-center HBs, he established a linear correlation; an increase in the covalent N–H bond length (d_{N-H}) implies a shorter $d_{H\cdots O}$. Furthermore for HBs with equal primary $d_{H\cdots O}$, the bond length d_{N-H} is significantly *longer* in a three-center (bifurcated) HB than in a two-center (or isolated) HB. The increase in the covalent N–H bond length is smaller in N–H···O bonds ($1.00\ \text{Å} < d_{N-H} < 1.08\ \text{Å}$) than in the equivalent O–H bond length in O–H···O bonds ($0.95\ \text{Å} < d_{O-H} < 1.20\ \text{Å}$).[20] However, it should be stressed that the lengthening of this bond is

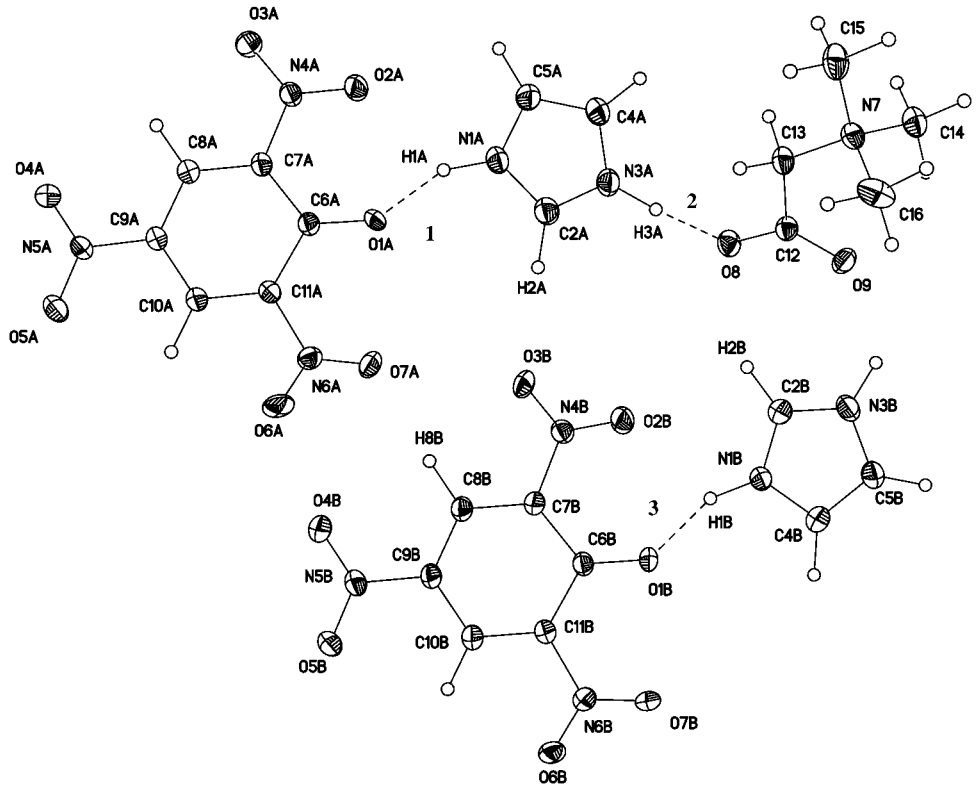

Figure 2. ORTEP drawing of **1** at 28 K with 90% probability surfaces shown.

Table 1. Selected N–H···O and C–H···O (A–H···O) bond lengths [Å] and angles [°].

Bond[a]		A–H	H···O	A···O	∢(A–H···O)
HB1	N1A–H1A···O1A	1.046(1)	1.630(1)	2.614(1)	154.6(1)
	H1A···O2A	2.315(1)			
HB2	N3A–H3A···O8	1.057(1)	1.635(1)	2.684(1)	171.0(1)
	H3A···O6A^{ii}	2.808(2)			
HB3	N1B–H1B···O1B	1.048(1)	1.681(1)	2.676(1)	157.0(1)
	H1B···O2B	2.236(1)			
	C8B–H8B···O7A	1.092(1)	2.167(1)	3.240(2)	167.0(1)
	C2A–H2A···O3B	1.092(1)	2.208(2)	3.296(2)	174.4(1)
	C2B–H2B···O8	1.077(1)	2.459(1)	3.384(2)	143.2(1)
	C2B–H2B···O2B	1.077(1)	2.577(1)	3.014(1)	105.4(1)

[a] symmetry operation ii: $0.5-x$, $0.5-y$, $-z$.

highly significant, since the analysis is based on neutron diffraction data. It is striking that d_{N-H}(HB2) is 0.011(1) Å longer than d_{N-H}(HB1) although $d_{H\cdots O}$(HB1) is 0.005(1) Å *shorter* than $d_{H\cdots O}$(HB2), as shown in Table 1. In addition d_{N-H}(HB1) may be further increased by bifurcation to O2A. Therefore the structural analysis indicates an anomaly in HB2 in comparison to well-established structural correlations. The structure also has a number of C–H···O interactions and the four shortest are listed in Table 1. The trends observed by Steiner[14] for N–H···O HBs appear to be valid for C–H···O HBs. A significant increase in d_{C-H} correlates with a shorter $d_{H\cdots O}$. The considerable strength of the two short C–H···O HBs suggests that they contribute significantly to the stabilization of the co-crystallized compound (see Table 3 later).

The resemblance of **1** to the catalytic triad in serine proteases may be assessed by a comparison of the structural features that are presented here with the structure of the catalytic triad as present in the native substrate-free *porcine pancreatic elastase* (PPP). A high-resolution ($d_{min}=1.1$ Å) X-ray crystallographic study of PPP has recently been published.[21] Here, the $d_{N\cdots O}$ between histidine and aspartate in the catalytic triad is found to be 2.70 ± 0.04 Å, which is similar to the bond length of 2.684(1) Å between N3A and O8 in **1** (HB2). A description of the transition-state configuration is obtained from an atomic resolution ($d_{min}=0.78$ Å) study of complexed *B. lensus subtilisin*.[22] Here the N···O separation between His and Asp in the catalytic triad is found to be 2.62(1) Å. Similar or slightly shorter distances are reported in a recent publication on the bonding in transition-state (TS) analogue complexes of chymotrypsin.[23] From the heteroatom distance (but not from $d_{H\cdots O}$) HB2 in the present complex appears to be intermediate between the "non-TS" structure of PPP and the "TS" structures of the *B. lensus subtilisin* and chymotrypsin complexes. The fact that HB2 is unusually strong, even in a "non-TS" configuration, indicates that this HB could be exceptionally strong in the real TS, in which the histidine and aspartate side chains are presumably closer together.

Topological analysis: Aspherical modeling of the experimental X-ray structure factors provides the total electron density distribution, $\rho(\mathbf{r})$, which is the main observable in the quantum theory of atoms in molecules (QTAM) developed by Bader and co-workers.[24] Table 2 lists the topological features at the bond critical points (bcp) of the short N–H···O and C–H···O interactions. The value of ρ_{bcp} for HB2 is greater than the corresponding values for HB1 and HB3; this

0947-6539/01/0717-3758 $ 17.50+.50/0 *Chem. Eur. J.* **2001**, *7*, No. 17

Table 2. Topology of the N–H···O and C–H···O HBs. The first line contains the experimental values, the second line the theoretical values.

Bond		ρ_{bcp} [e Å^{-3}]	$\nabla^2\rho_{bcp}$, [e Å^{-5}]	d_{1-bcp} [Å]	d_{2-bcp} [Å]
HB1	O1A···H1A	0.360(34)	3.58(9)	1.089	0.541
		0.347	3.70	1.100	0.532
	N1A–H1A	2.009	–28.4(5)	0.786	0.261
		2.029	–42.0	0.810	0.234
HB2	O8···H3A	0.399(33)	1.93(9)	1.094	0.545
		0.366	3.39	1.110	0.531
	N3A–H3A	1.930(65)	–30.5(5)	0.804	0.254
		2.004	–37.4	0.805	0.249
HB3	O1B···H1B	0.289(33)	3.29(8)	1.128	0.556
		0.309	3.34	1.127	0.553
	N1B–H1B	2.043(65)	–31.7(5)	0.785	0.263
		2.028	–41.8	0.810	0.235
	C8B–H8B	1.848(55)	–19.7(3)	0.756	0.337
		1.929	–24.6	0.727	0.360
	O7A···H8B	0.102(15)	1.49(2)	1.334	0.834
		0.102	1.34	1.352	0.821
	C2A–H2A	1.912(57)	–23.9(3)	0.734	0.358
		1.957	–25.8	0.730	0.352
	O3B···H2A	0.087(17)	1.13(2)	1.379	0.829
		0.094	1.17	1.392	0.815
	C2B–H2B	1.925(56)	–23.6(3)	0.746	0.331
		1.971	–25.9	0.723	0.355
	O8···H2B	0.059(6)	0.90(1)	1.489	0.973
		0.064	0.74	1.499	0.954
	O2B···H2B	0.049(7)	0.91(1)	1.454	1.178
		0.052	0.81	1.457	1.145

indicates an increased accumulation of charge in HB2. The Laplacian, $\nabla^2\rho_{bcp}$, for HB2 is less positive than for HB1 and HB3; this also indicates an increased covalence in this bond. At the same time, the lower value of ρ_{bcp} for N3A–H3A than for N1A–H1A and N1B–H1B illustrates the accompanying weakening of the covalent N–H interaction in HB2. These observations corroborate the structural findings that were discussed above, and the EDD supports the observed anomaly in the correlation between d_{N-H} and $d_{H\cdots O}$. This is evident in Figure 3, in which the Laplacian of the electron density in the planes of the three N–H···O HBs is shown. The polarization of the Laplacian around H3A towards O8 in HB2 is pronounced in comparison to the other two HBs. Such a polarization of charge is unexpected for "normal" electrostatic HBs and suggests that HB2 is intermediate between a normal HB and an LBHB. The features of the Laplacian of an LBHB[6] are characterized by a hydrogen atom that is almost symmetrically positioned between two heteroatoms with its charge distribution polarized towards both. Since H3A in this complex retains the strong covalent interaction with N3A, HB2 is not an LBHB, though the polarization of H3A towards the acceptor atom, O8, does resemble the polarization that would be observed in an LBHB. This polarization is modeled with large and highly significant quadrupolar electron-density functions on the hydrogen (Q_{2+}(H3A) = 0.113(21)). If such functions are not included in the multipole refinement, the polarization disappears. This subtle point is quite important because it shows that models commonly used in both experimental and theoretical studies of strong HBs may not be adequate. Theoretically, it is common practice to include p orbitals (polarization functions) on the hydrogens. However, p functions may not model this feature in HB2, which could require orbitals of higher angular momentum. Indeed, Figure 4 (middle) shows that single-point calculation on **1** at the B3LYP/6–311G(d,p) level does not decribe the large polarization of HB2. A systematic study of theoretical-basis-set limitations is beyond the scope of the present paper, but the experimental data suggest that accurate theoretical studies of strong hydrogen bonds should include d orbitals on the essential hydrogen atoms.

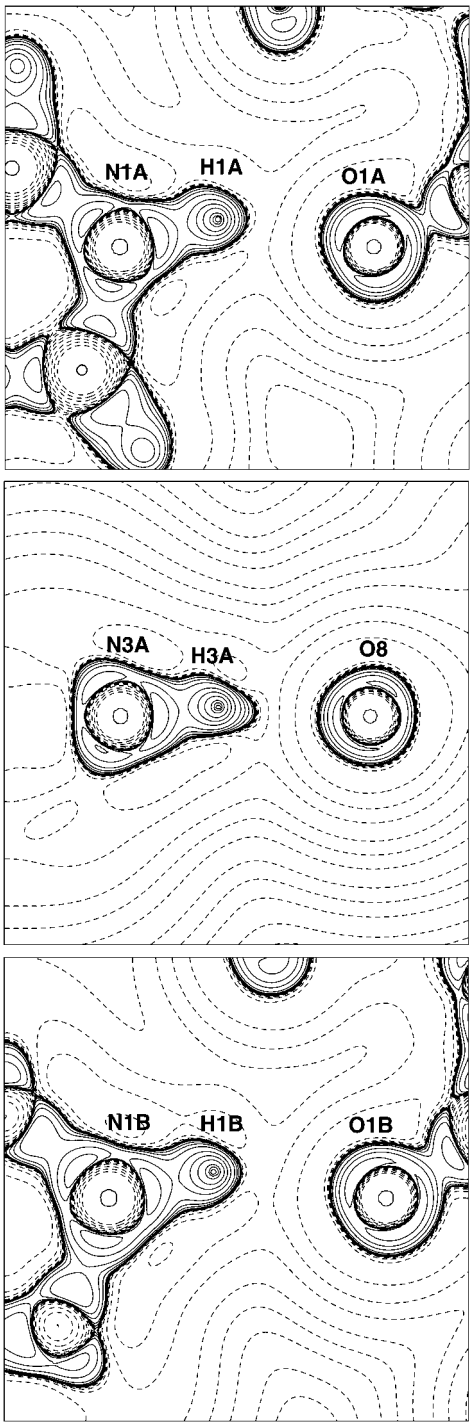

Figure 3. Contour plot of the negative of the Laplacian of the electron density in the planes of the three strong N–H···O HB's in **1**. Top) HB1; middle) HB2; bottom) HB3. Contours are drawn at 1, 2, 4, 8×10^n, $n = -3$, -2,…, 1, 2. Solid lines are positive contours, broken lines negative.

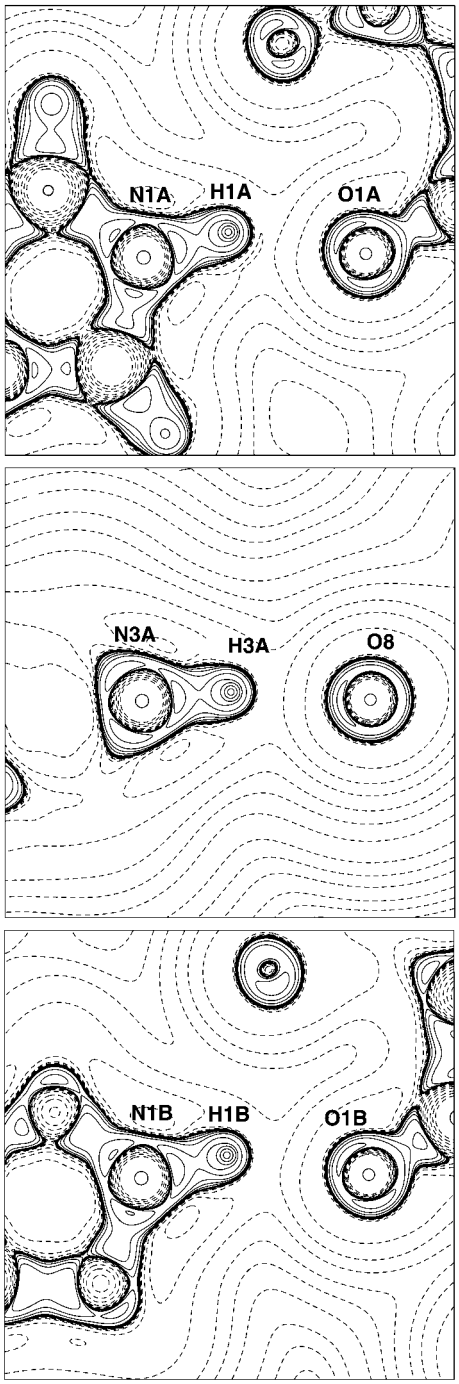

Figure 4. Laplacian of the theoretical density. Plots and contours as in Figure 3.

Table 3 lists HB energies calculated from a) the Abramov functional,[25] b) a structural correlation with $d_{H\cdots O}$,[11a] c) a topological correlation,[11b,c] and d) the theoretical wave function using AIMPAC.[26] Estimates of the HB energies are calculated by using the empirical relation $E_{HB} = -1/2\,V$,[11a] in which V, the potential energy density, can be obtained either directly, as in d), or calculated from the virial theorem and the topology, as in a) and c). By all methods of evaluation, HB3 is the weakest of the three N–H···O HBs, although an E_{HB} of approximately 13 kcal mol^{-1} is still quite a strong interaction. Both HB1 and HB2 are found to be

Table 3. Hydrogen-bond energies (E_{HB}) obtained as $E_{HB} = -1/2\,V$[11c], in which V is the potential energy density, and from ab initio theory. E_{HB} is given in kcal mol^{-1}.

Bond	E_{HB}[a]	E_{HB}[b]	E_{HB}[c]	E_{HB}[d]
HB1	17.5	16.9	20.5	16.1
HB2	18.3	16.6	24.6	16.5
HB3	13.0	14.1	16.1	13.5
N3B–H3B···O9	4.1	3.2	3.3	4.2
C8B–H8B···O7A	3.3	2.4	3.6	5.8
C2A–H2A···O3B	2.5	2.1	3.4	5.0
C2B–H2B···O8	1.7	0.9	1.4	3.5

[a] Method: the Abramov functional.[25] [b] Method: a structural correlation with $d_{H\cdots O}$.[11b] [c] Method: a topological correlation.[11a,c] [d] Method: V obtained directly from the theoretical wavefunction.[26]

stronger HBs and according to the definitions which are often used for E_{HB}, they could be designated as LBHB;[3] however, in this case, as discussed above, they are not. It is important to stress that an HB can have considerable strength, although it is not an LBHB. The anomaly, which is observed in the structural correlation of bond length and bond strength, becomes apparent as the method b) fails to produce the same rank of HB strength as the other methods. The difference between E_{HB}(HB1) and E_{HB}(HB2) is small and likely insignificant, although the characteristics of the structure and the EDD indicates that HB2 is the strongest bond. The semi-empirical Abramov expression (a) is based on closed-shell interactions[24] and does not properly account for the increased covalency of HB2. Even so, HB2 is found to be the strongest bond. The theoretical calculation (d) also neglects some of the increased covalence of HB2 and this makes the difference in strength between HB1 and HB2 quite small.

In order to assess the reliability of the empirical estimates of the HB strengths, we have attempted to estimate E_{HB} for HB2 using DFT calculations. For hydrogen bonds with large covalent contributions, for example, as in benzoylacetone[6] and nitromalonamide,[16b] the empirical estimates may have large errors. Thus, the empirical charge density estimates are around 50 kcal mol^{-1} for both molecules in comparison to ab initio theoretical estimates of 16 kcal mol^{-1} and 27 kcal mol^{-1} for benzoylacetone and nitromalonamide, respectively. Theoretically, HB strength can be estimated by comparing the total energy of the system with the energy of rotameric structures[6] or with systems that have donor and acceptor groups which are separated to infinity. Such procedures assume that the HB in question is the only interaction between the fragments. This may be a crude approximation in complicated structures such as **1**. To obtain an estimate of E_{HB} for HB2 we use the neutron geometry to calculate the total energy of fragment A, that is, the upper picric acid, imidazole, and betaine molecules shown in Figure 2 (fragment B is depicted in the lower part). This energy is then compared to the sum of the total energies from a partial geometry optimization of a picric acid/imidazole dimer and a betaine molecule. Both structures are fixed at the neutron geometry apart from the atoms that are involved in HB2, which are allowed to relax after the two fragments are cut apart. In this approach, we assume that all fragments making up the crystal suffer equally from being cut out of the crystal environment.

  0947-6539/01/0717-3760 $ 17.50+.50/0

We carried out some calculations to validate the procedure, for example, the atoms in fragment A which point towards fragment B were allowed to relax, but this only changed the energy by about 0.5 kcal mol^{-1}. The estimated bonding energy for HB2 is 21 kcal mol^{-1}, a value which is in excellent agreement with the results obtained from the experimental CD. The theoretical calculation furthermore gives an interaction energy of 16 kcal mol^{-1} between fragments A and B. The comparable value from the experimental CD is the sum of the four intermolecular hydrogen bonds between these fragments. Their individual values are given in the lower part of Table 3 and their sum varies between 9 and 19 kcal mol^{-1} for the different types of estimates. The individual energies of these HBs cannot be calculated theoretically due to the complex network of intermolecular interactions present in the crystal.

Comparison between experiment and theory: The transferability of atomic fragments or functional groups between different molecular systems is a central concept in chemistry.[23] The most comprehensive experimental EDD studies of transferability have been carried out by Lecomte and coworkers, who focus on building charge density libraries of peptide fragments in order to construct large polypeptide systems.[27] In such studies, it is important to know how transferable a given unit is between different systems and if possible, to discover how units are perturbed by their surroundings. This is difficult because the comparison of a given unit in two different crystal systems is affected by differences in the systematic errors in the two experiments. Thus observed differences between two units may be due to differences in the chemical surroundings as well as systematic errors in the experiments. The transferability of a given group can be better assessed if several different units are present in the same crystal structure, since systematic errors are (presumably) identical. The present complex offers the opportunity to compare different imidazoles and picric acids by using topological methods.

In the case of fully covalent homoatomic C–C bonds, the correlation between experimental and theoretical results is outstanding with quantitative agreement (see Table 4). However, as the bonds become more polar, that is, C–H, C–N, and N–O, there is increasing discrepancy. For N–O, theory predicts average values of $\rho_{bcp} = 3.32(6)$ and $\nabla^2\rho_{bcp} = -24.3(1.3)$ whereas experiment gives $\rho_{bcp} = 3.28(8)$ and $\nabla^2\rho_{bcp} = -12.1(2.5)$. There is a tendency in theory to give more negative values for $\nabla^2\rho_{bcp}$ in polar bonds, whereas ρ_{bcp} is almost perfectly matched. This tendency is further substantiated in the C–N bonds, in which the agreement improves as multiple bond character increases. On the other hand, hydrogen bonds show good correspondence. It appears that in the limits of either full covalency or closed-shell interactions the experimental and theoretical results agree well, but for intermediate-bond types the differences are larger. In previous studies, it has been observed that both experiment and theory may have difficulties in describing the diffuse bonding regions.[28] In the case of the X-ray method, it was found that the radial functions, which are commonly used in the multipole model, can be too rigid and can introduce model bias in the experimental densities. It is interesting to note that the spread of individual bond types is smaller for theory than for experiment. This is seen in the values of $\nabla^2\rho_{bcp}$, d_{1-bcp}, and d_{2-bcp} of the polar bonds. The different spreads may reflect real differences among the crystal bonds, which are not modeled by theory. The larger experimental spread of the C–C bonds suggests that the effect is at least partly due to real differences in the surroundings.

Table 4. Comparison of the theoretical and the experimental topology. In square brackets the number of bonds included in the averages are listed. The first line contains the experimental values, the second line the theoretical values with standard uncertainty calculated as sample esd. "be" short for betaine, "pa" short for picric acid.

Bond	$\langle\rho_{bcp}\rangle$ [e Å^{-3}]	$\langle\nabla^2\rho_{bcp}\rangle$ [e Å^{-5}]	$\langle r_{1-bcp}\rangle$ [Å]	$\langle r_{2-bcp}\rangle$ [Å]	$\langle R_{ij}\rangle$ [Å]
$(C-C)_{pa}$[8]	2.15(5)	−21.5(7)	0.68(4)	0.71(4)	1.385(9)
	2.13(3)	−21.5(4)	0.69(1)	0.691(9)	1.383(8)
$(C-C)_{pa}$[4]	1.90(2)	−16.5(6)	0.70(3)	0.75(3)	1.458(4)
	1.89(2)	−17.4(3)	0.715(2)	0.740(4)	1.455(5)
$(C-H)_{be}$[11]	1.85(4)	−19.1(13)	0.69(2)	0.39(2)	1.086(7)
	1.91(4)	−23.6(9)	0.705(5)	0.383(8)	1.089(8)
$(C-N)_{pa}$[6]	1.79(6)	−16.0(12)	0.90(3)	0.55(3)	1.450(8)
	1.81(3)	−16.5(9)	0.908(8)	0.540(8)	1.449(6)
$(C-N)_{be}$[4]	1.60(3)	−10.0(9)	0.88(1)	0.62(1)	1.500(4)
	1.62(2)	−13.7(4)	0.924(6)	0.574(7)	1.499(5)
$(N-O)_{pa}$[12]	3.28(8)	−12.1(25)	0.64(1)	0.59(1)	1.233(9)
	3.32(6)	−24.3(13)	0.643(2)	0.587(5)	1.231(7)

The origin of LBHB: Our central question, which remains unanswered, is what causes the formation of a LBHB? It is not merely the donor–acceptor distance that determines the HB type. As mentioned above, citrinin has a localized HB,[15] while benzoylacetone exhibits a LBHB[6] although their O···O bond lengths are almost identical. There must be environmental effects that change the potential energy surface of the hydrogen atom. One could also ask which differences in the chemical environment in and around the strong N–H···O HBs in **1** make HB2 stronger than the shorter HB1. We have so far described the structural and topological features of the three HBs in **1** and we will now examine how the surroundings affect the HB character. This can be done by evaluating Green's function for the density, which is also called the source function (S) and which was recently developed by Gatti and Bader.[19] This concept is based on the fact that the value of the electron density at any point in space may be separated into a sum of atomic contributions from every atom within the molecule. The source function has so far been encoded only for use with theoretical wavefunctions.[19] To probe the potential use of this function in analysis of hydrogen bonding, the source function values at the bcps of HB1, HB2, and HB3 are calculated by using the wavefunction from the theoretical calculation. For comparison, we also calculated the source function for two smaller molecules, which are examples of an LBHB: benzoylacetone[6] (see Figure 5) and a single-well HB, nitromalonamide,[16b] respectively (see Figure 6). The theoretical calculations on these two molecules have been published in papers that describe accurate low-temperature diffraction experiments.[6, 16b] The combination of the different studies cover the complete range of strong HBs (localized HB, LBHB, and single-well HB).

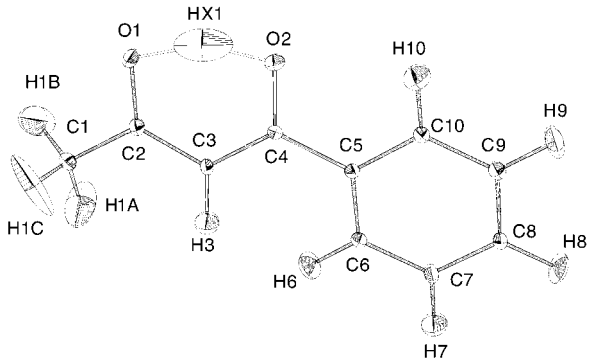

Figure 5. ORTEP drawing of benzoylacetone, shown with 50% probability ellipsoids.

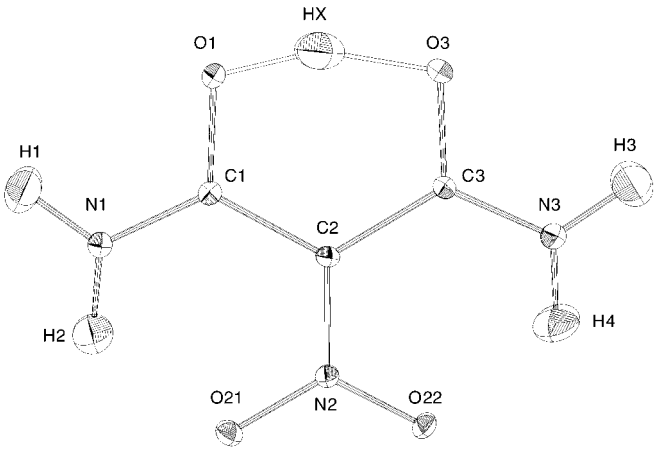

Figure 6. ORTEP drawing of nitromalonamide, shown with 50% probability ellipsoids.

There are different ways to determine the reliability of the source function. The integrated charge must sum to the total number of electrons in the complex. Furthermore, the sum of S over all atoms at the bcps must equal the values that are obtained from a topological analysis of the density. These criteria were fulfilled to within 1% for all three HBs, and the results are listed in Tables S1–S3 in the Supporting Information and are visualized in Figures 7, 8, and 9. The part of the density at the bond critical point, ρ_{bcp}, contributed by the hydrogen that is involved in the HB, is very different for the different HBs. For HB3, the weakest of the three HBs in **1**, the contribution is negative (-0.0071 e Å^{-3}) and amounts to ($-$)2% of the total density at the bcp. The hydrogen contribution is positive for the other HBs and increases rapidly as the hydrogen becomes more delocalized. This correlates with results from a theoretical study of a water dimer, in which the source contribution from the hydrogen is negative at the equilibrium geometry but increases and becomes positive at an O$\cdots$O separation of less than 2.4 Å.[29] A large increase in the source contribution from the hydrogen (S(H)) to the density at the bcp is observed in benzoylacetone and nitromalonamide, as shown in Figures 10 and 11, respectively. Here, the hydrogens account for more than 30% of the total electron density at the bcps. Of course, the contribution from hydrogen is dependent on d_{H-bcp}, which decreases as $d_{H\cdots O}$ is shortened. Nevertheless, for HB1 in **1**, d_{H-bcp} is 0.532 Å in comparison to 0.531 Å in HB2. This insignificant difference does not explain the observed increase (from 0.0038 e Å^{-3} to 0.0181 e Å^{-3}) in S(H). Therefore it must be electron distribution in the hydrogen atoms that has changed, and this confirms that HB2 differs from HB1. This result is obtained irrespective of the fact that the theoretical density does not contain all the experimentally observed polarization in HB2 (see above). Similarly, S(H) in the single-well HB in nitromalonamide is 0.1924 e Å^{-3} ($d_{H-bcp} = 0.360$ Å) in comparison to 0.2655 e Å^{-3} in the LBHB of benzoylacetone ($d_{H-bcp} =$ 0.350 Å). The decrease in d_{H-bcp} of 3% from nitromalonamide to benzoylacetone does not explain the increase of 38% in source contribution from the hydrogen. It appears that there are differences between the systems that induce large changes in the hydrogen source contribution.

The three donor–hydrogen–acceptor atoms contribute more than 85% of the total density at the bcp in the low-barrier and single-well HBs in comparison to between 55 and

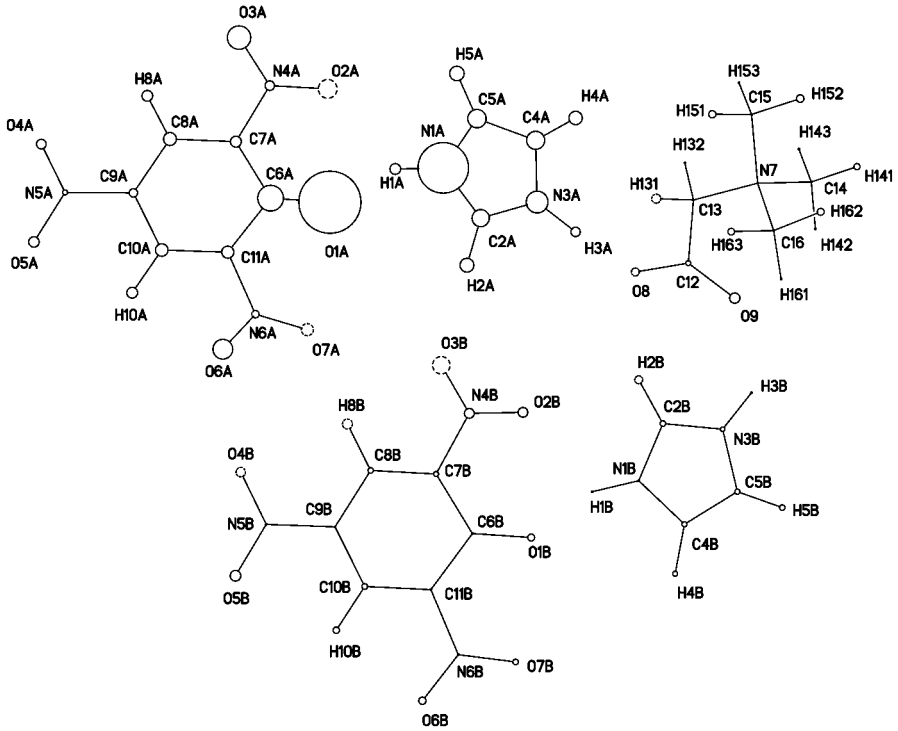

Figure 7. Source contributions to HB1 in **1**. For every atom, the size of the circle is proportional to the source contribution from that atom. Positive contributions are indicated with full circles, negative contributions with dashed circles. Contributions of less than 7×10^{-4} e Å^{-3} are not shown.

0947-6539/01/0717-3762 $ 17.50+.50/0 *Chem. Eur. J.* **2001**, *7*, No. 17

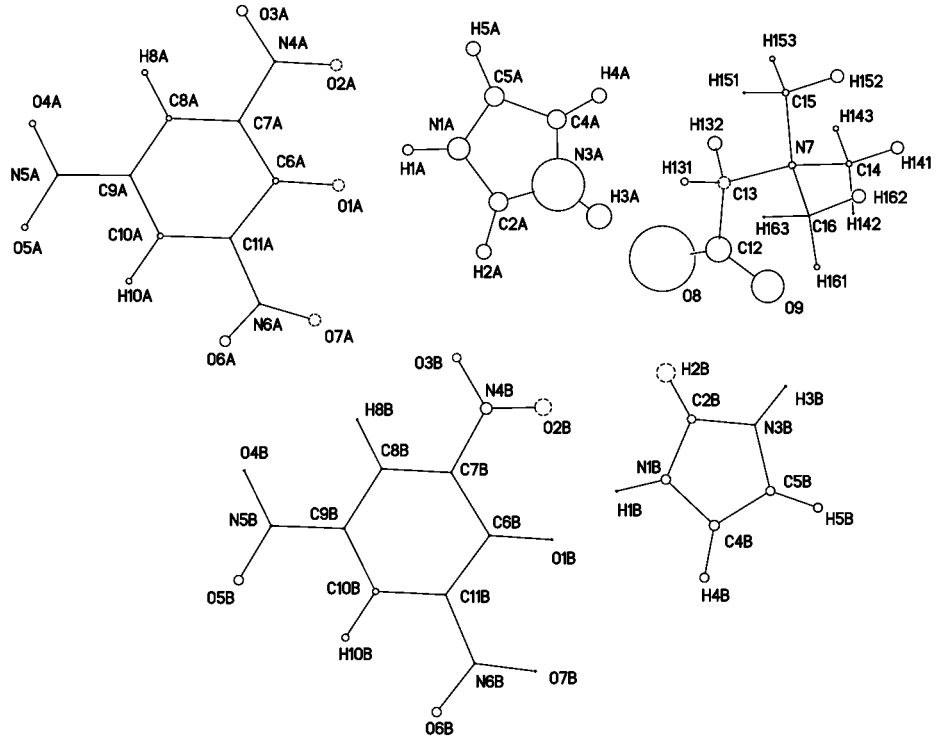

Figure 8. Source contributions to HB2 in **1**. Features as in Figure 7.

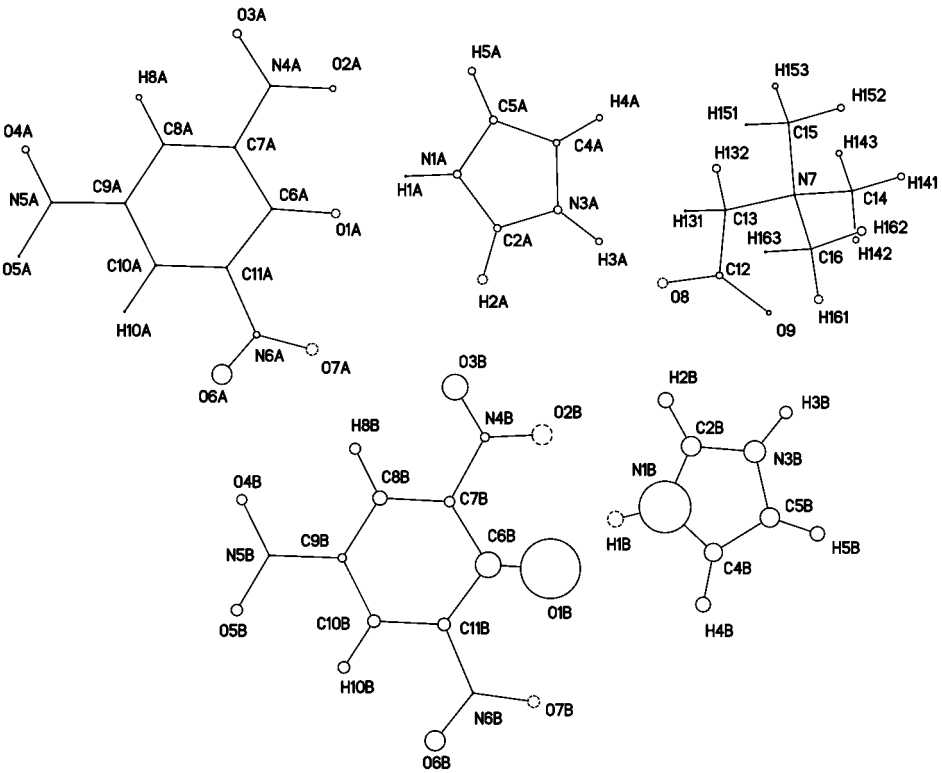

Figure 9. Source contributions to HB3 in **1**. Features as in Figure 7.

62 % in the localized HBs in complex **1**. However, the sum of the source contributions from the donor and the acceptor atoms seems almost unaffected by the HB type. This sum is in a narrow range from 56 % to 61 %, and the values of the three localized N–H···O HBs from this study cluster around 57 %. This seems to be valid even in the extreme case of covalent HBs. Thus, the main change when approaching the LBHB state is in the hydrogen atom source contribution, as the contributions from the surroundings are relatively unchanged. It is not evident from the present data alone what causes LBHB formation. If, for example, release of steric strain in benzoylacetone contributes to LBHB formation,[6a] then the source contributions to the bonds must be evaluated at other points of the potential energy surface than merely the equilibrium geometry.

A signature of an LBHB is a very large ^{1}H NMR chemical shift.[2f] If the three types of strong HBs (localized HBs in **1**, LBHB in benzoylacetone, single-well HB in nitromalonamide) are compared, the ^{1}H NMR chemical shift is observed to increase from a broad peak value of $\delta = 14.8$ in **1** to $\delta = 16.3$ for the LBHB system of benzoylacetone and then to decrease to $\delta = 14.4$ in nitromalonamide as the system becomes compressed.[30, 31] This trend was also observed by Madsen et al[16b] for the hydrogen atomic displacement parameters (ADPs) along the O···O direction. Thus, hydrogen ADPs increase dramatically as the system becomes an LBHB, but decrease with further compression of the potential well. The source function behaves similarly as the ^{1}H NMR chemical shifts and hydrogen ADPs with a maximum value at LBHB. This suggests that the source function may quantify the reason that ^{1}H NMR chemical shifts are sensitive to the character of a hydrogen bond.

The heteroatom separation ($d_{N\cdots O}$) in **1** is shorter than the value observed in a non-transition-state structure of a serine protease[21] and is of similar length or slightly longer than stable inhibitor complexes that mimic the transition state.[23] However, we note that only $d_{H\cdots O}$ is a truly relevant parameter,

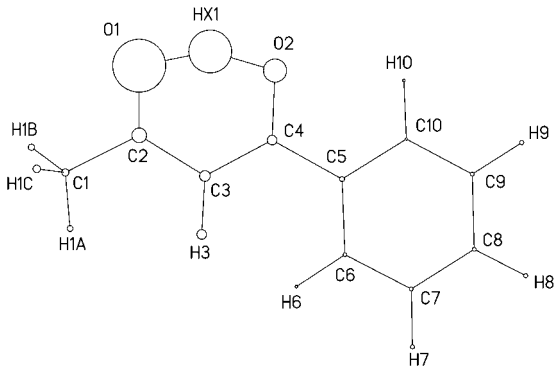

Figure 10. Source contributions to HB(O1) in benzoylacetone. Features as in Figure 7.

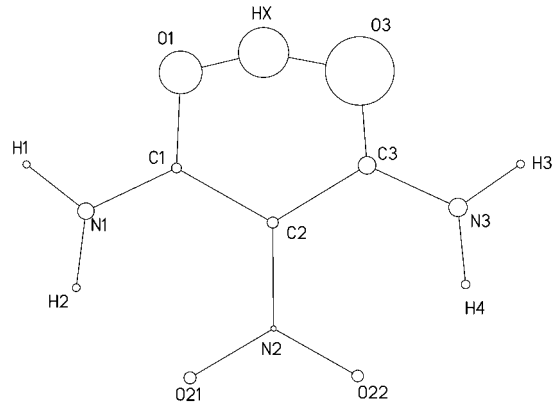

Figure 11. Source contributions to HB(O3) in nitromalonamide. Features as in Figure 7.

and this distance is not available from protein crystallographic studies. In the TS, $d_{N\cdots O}$ is supposedly further shortened relative to the values found in **1**, and this must lead to an increase in the strength of the HB, which in serine proteases would be analogous to HB2 in the model system. Since HB2 is already strong, we may expect that the hydrogen bond energy in the TS is substantial. Furthermore, if it is the TS stabilization energy obtained from the HB (i.e., not the nature of the HB) that is important for enzyme catalysis, the present study suggests that discussions on this subject may overemphasize the importance of HB character and whether ot not an actual LBHB is involved. The present study shows that localized HBs can be strong. Hence, an LBHB may be a sufficient but not a necessary condition for enzyme catalysis from an energetic point of view.[32] However, there are extensive spectroscopic data[33] that indicate the existence of an LBHB between His57 and Asp102 in the TS of the catalytic triad. Systematic studies that employ tools like the source function may enable us to further probe the nature of very short hydrogen bonds and to understand how chemical environments could induce LBHB formation.

Conclusion

We show that the nature and strength of an HB are not unambiguously determined by the geometrical parameters which define the system. Topological analysis of the experimentally determined EDD reveals that a localized HB, which is dominated by electrostatic interactions, can have considerable strength. One such bond in complex **1**, HB2, appears to be intermediate between a localized and a delocalized HB with a polarized charge distribution towards the acceptor atom. The experimental bond energies of the HBs in **1** exceed the generally accepted threshold for an LBHB although all three hydrogen atoms are localized in nitrogen wells. This suggests that LBHB is a sufficient but not a necessary condition for TS stabilization in the catalytic triad. The source function was introduced to analyse strong HBs. This concept elucidates the role of the hydrogen atom EDD in the bonding. It appears that the main change on the formation of an LBHB is a dramatic increase in the hydrogen atom source contribution to the HB, whereas the changes in the contributions from the surroundings are subtle. More systematic studies of similar systems are required to quantify these changes. Ultimately, such studies may give us a *chemical understanding* of the shape of the potential energy surface in an HB.

Experimental Section

Neutron data: The main purpose of the neutron diffraction study was to establish an unbiased structural model for the hydrogen atoms, which are the crucial entities of the study. Secondly, neutron refinements can probe the hydrogen thermal displacements for possible anharmonic components, which indicate the shape of the potential energy surface. The neutron measurements were carried out at the SCD beam line at the Intense Pulsed Neutron Source, Argonne National Laboratory. A yellow crystal of dimensions $2.0 \times 2.2 \times 3.0$ mm was wrapped tightly in aluminum foil and fastened on an aluminum pin with tiny amounts of glue on the foil. The aluminum pin holding the sample was fitted on the cold station of a type CS-202 Displex refrigerator, which was mounted on a type 512 Huber four-circle diffractometer. This device employed the white beam of a spallation source, and the diffractometer was also equipped with a position-sensitive area detector.[34] The speed of the SCD instrument was vital in the present study in order to obtain high-resolution data within strict beam time limitations on a large unit cell structure of 75 unique atoms. The instrument had ω fixed at 45°, and different volumes of reciprocal space were recorded by setting ϕ and χ at a number of values. A total of 32 three-dimensional data histograms (x and y spatial coordinates on the detector and the time of flight, t) were recorded during two weeks of data collection. Reflections were restricted to those in which the wavelength of the neutrons was between 0.7 and 4.2 Å. The temperature was fixed at 28(1) K in order to match the temperature used in the synchrotron X-ray experiment. Further experimental details for the neutron study are listed in Table 5. Crystallographic data (excluding structure factors) for the structures reported in this paper have been deposited with the Cambridge Crystallographic Data Centre as supplementary publication no. CCDC-112286. Copies of the data can be obtained free of charge on application to CCDC, 12 Union Road, Cambridge CB2 1EZ, UK (fax: (+44) 1223-336-033; e-mail: deposit@ccdc.cam.ac.uk).

Local Argonne programs were used in all steps of the data acquisition, data reduction and structure refinement.[35] The first set of programs searched for intensity maxima in the histograms, indexed the peaks, and refined an orientation matrix. The peak intensities were integrated by using a two-dimensional Lehmann–Larsen type box integration.[36] The algorithm located the integration rectangle which yielded the minimum $\sigma(I)/I$ value in the spatial direction, and up to five time-slices were then added to obtain a minimum $\sigma(I)/I$ for the total peak. The intensities were corrected for the Lorentz factor and normalized according to the known spectral distribution of the incident beam and detector efficiency. The data were also corrected for absorption by using a spherical crystal approximation. Neutron scattering lengths and absorption cross sections were taken from Sears.[37] For hydrogen, cross sections measured by Howard et al were used.[38]

0947-6539/01/0717-3764 $ 17.50+.50/0 *Chem. Eur. J.* **2001**, *7*, No. 17

Table 5. Experimental details for the crystallographic measurements on the co-crystal of $C_5NO_2H_{11}$, $C_3N_2H_5$, and $C_6N_3O_7H_2$ ($C_{23}N_{11}O_{16}H_{25}$ in the asymmetric unit, $M_r = 711.51\ g\,mol^{-1}$).

	Tube	Synchrotron	Neutron
T [K]	10(1)	28(1)	28(1)
λ [Å]	0.5608 ($Ag_{K\alpha}$)	0.643(1) (Si(100))	0.7–4.2 (white beam)
a [Å]	33.57(1)	33.54(2)	33.536(5)
b [Å]	7.640(2)	7.64(2)	7.636(1)
c [Å]	25.031(8)	24.98(4)	25.066(4)
β [°]	114.84(2)	114.76(5)	114.90(1)
V [Å^3]	5826(6)	5813(30)	5822(2)
space Group	$C2/c$	$C2/c$	$C2/c$
Z	8	8	8
$V_{crystal}$ [mm^3]	0.058	0.001	13.2
μ_L [cm^{-1}]	0.06 (no correction)	0.08 (no correction)	1.22 (μ_a) 1.15 (μ_s)
reflections measured	16382	98132	29014
unique reflections	3187	15657	
R_{int}	0.016	0.030	
$(\sin\theta/\lambda)_{max}$ [Å^{-1}]	0.51	1.08	1.30 (partial data) 0.81 (complete data)
observed reflections	11182		8867 [$I > 3\sigma(I)$]
parameters	1128		708
$R(F)$	0.035		0.082
$R(F^2)$	0.046		0.063
S	1.13		1.79

"Equivalent" reflections could not be averaged as they were recorded at different wavelengths which, for example, leads to differences in extinction

Synchrotron X-ray data: The synchrotron data were collected at beam line X3A1 at the National Synchrotron Light Source at Brookhaven National Laboratory (USA). A nearly spherical crystal with a diameter of 0.12 mm was mounted with epoxy glue to thermally conducting carbon fibers and connected to a brass pin via a copper wire. This arrangement was placed directly on the cold finger of a type 201 Displex refrigerator fitted inside the Be-vacuum cup. An antiscatter device was used to reduce parasitic scattering.[39] The diffracted radiation was detected with image plates (IP) which have an active area of 250×400 mm^2. The IPs were scanned offline with a FUJI BAS2000 scanner with a pixel size of 0.1×0.1 mm^2 and a dynamic range of 10^4. Further details of the experimental conditions are given in Table 5. Good coverage of the reciprocal space was achieved by using five different combinations of crystal–detector distance (cm) and 2θ angles (°) for the IP's [$(d,2\theta) = (15.0, 0)$, $(20.0, 0)$, $(30.0, 0)$, $(20.0, 40)$, $(30.0, 50)$]. For each setting an orientation matrix was extracted by using DENZO.[40] Integrated intensities were subsequently obtained with the HIPPO program,[41] which uses the seed skewness method to define the individual peak size. Only fully observed reflections were accepted for subsequent refinement. Since the diffracted X-rays travel different distances through the detector a 2θ-dependent intensity correction was carried out.[42] A total of 98132 intensities from 298 IP's were scaled and averaged using SORTAV.[43] The refined scale factors for each separate plate were found to accurately display the beam decay. The averaging procedure removed approximately 22000 outlier reflections, and the remaining reflections were reduced to 15657 unique reflections with an average redundancy of 4.9 and an internal agreement of 3.0%. Owing to the requirement of the antiscatter device, the data set suffered from a few missing reflections in the low-order region. It was therefore decided to supplement the synchrotron data with low-order data from a conventional X-ray experiment.

Conventional X-ray data: A spherical crystal with a diameter of 0.48 mm was mounted on the tip of a glass fiber and attached to a brass pin. This was fitted directly on the cold finger of a type 202 Displex closed-cycle refrigerator, which was mounted on a HUBER type 512 four-circle diffractometer at the University of Aarhus. The vacuum around the crystal was closed by three thin-walled Be-cups. The crystal was cooled to 10(1) K and data were collected with $Ag_{K\alpha}$ radiation ($\lambda = 0.5608$ Å). The orientation matrix was determined from 29 reflections. Repeated measurement of three intense low order reflections ($hkl = 002$, 602, -402) every 50 reflections ensured a reliable evaluation of beam instability and crystal decay. A complete hemisphere of data with $\sin\theta/\lambda < 0.51$ Å^{-1} was measured in five weeks. Integrated intensities were extracted with program COLL5N, which uses the $\sigma(I)/I$ criteria to separate the peak from the background.[36] The program DATAP was used for normalization of the intensities based on the standard reflections.[44] Both absorption and extinction was found to be negligible. The 16382 measured reflections were averaged by the program SORTAV[43] and reduced to 3178 unique reflections with an average redundancy of 4.7 and an internal agreement of 1.6%.

DFT calculations: The DFT calculations were performed with the Gaussian 94 and Gaussian 98 suite of programs.[45] Single-point calculations in the neutron geometry were carried out at the B3LYP/6–311G(d,p) level of theory. This basis set has been found to be a good compromise between accuracy of calculation and cost of computation.[13] Many of the calculations mentioned in the introduction were carried out at a similar or lower level of theory.[7, 8] Analysis of the electron density was performed within the framework of the quantum theory of atoms in molecules (QTAM)[23] by using the AIMPAC programs,[25] which were locally modified to handle the large size of the system. The neutron geometry used in the calculations is only slightly different from the geometry obtained with the partial X–N refinement procedure due to small differences in the systematic errors between the X-ray and neutron data sets. The mean deviation in the bond lengths between the neutron and the X–N structures is 0.0029(2) Å for 82 bonds (including all HB's). This corresponds to about 2 esds on the individual bond lengths and it is much smaller than the accuracy that can be obtained in a theoretical geometry optimization. The difference in geometry therefore has negligible influence on the comparison of the two densities.

Neutron refinements: The refinement began with a room temperature X-ray structure.[46] The refined structure gave an unsatisfactory correspondence between the atomic displacement parameters (ADPs) determined from the X-ray data and the neutron ADPs. The origin of the discrepancy was found to be poor integration of some of the very high order neutron data; this was caused by peak overlap along the two short reciprocal axes. In subsequent refinements data with $H > 34$ and $L > 25$ were removed. The final refinement also employed a robustness criterion, which multiplies the minimum of (F_o/F_c, F_c/F_o) on the least-squares weights and thereby downweights outliers in the refinement. In our previous accurate neutron diffraction studies[6] refinement of anharmonic thermal parameters was used to obtain information about the shape of the hydrogen potential energy surfaces.[6, 16] In the present case, none of the hydrogens had significant (2σ level) third-order Gram–Charlier parameters. None of the hydrogens involved in HBs moved more anisotropically than the other hydrogens in the structure; this indicates that even the hydrogens involved in the short N–H···O contacts are firmly localized in their "nitrogen well".

X-ray refinement: In the X-ray refinements, the two data sets were co-refined. This was possible because atomic motion at 10 K and 28 K is close to zero-point vibration values and because the thermal smearing has very limited effect on the low-order data. Furthermore, extinction, which is wavelength dependent, was found to be negligible for both crystals. Careful comparisons of the two X-ray data sets revealed that singly or doubly measured reflections measured with the IP technique sometimes contain very poorly fitted data, which could not be spotted by an averaging procedure.[47] Therefore only structure factors that were based on three or more observations were used. Even among the multiple measured data, there are a few severe outliers. These reflections were identified through a model-dependent rejection scheme. Thus structure factors with $|F_o - F_c| / \sigma(F_o) > 10$, $F_o/F_c > 5$ or $F_o/F_c < 0.2$ were removed. In the rejection scheme F_c was based on an independent atom model refinement. This procedure resulted in a final data set of 8099 synchrotron and 3083 tube reflections. There are 2558 common data and 525 reflections unique to the tube data.

The electron density distribution (EDD) was modeled with the Hansen–Coppens formalism[48] with the XD program package.[49] The refined neutron structural model was adopted as the initial structure and the more accurate neutron unit-cell dimensions were used. The hydrogen positions and ADPs were fixed at neutron values. The multipoles were truncated at the octupolar level for all non-hydrogen atoms. Hydrogens, which are involved in hydrogen bonding, were modeled by using all dipoles and quadrupoles, while the remaining hydrogens were refined with one bond-directed dipole and one quadrupole (d_{z^2}). For each atom type the radial

functions were adjusted by refinement of one κ' for the spherical valence shells and one κ_l'' for the multipoles (six kappa sets).

Inspection of the refined multipole parameters revealed that the data reflect the expected local non-crystallographic mirror symmetry on the four-ring systems. Thus only two parameters that violate the mirror symmetry were significant at a 2σ level. This supports the idea of introduction chemical constraints in cases of limited data set or in non-centrosymmetric structures.[50] However, the extent and accuracy of the present data allowed unconstrained refinement of all parameters. An indication of the data quality was obtained from the comparison of ADPs obtained independently from X-ray and neutron refinements.[51] The ADPs can absorb uncorrected systematic errors and a good agreement between the ADPs from a neutron experiment and a multipolar modeling of X-ray data therefore implies that systematic errors have been minimized. The non-hydrogen ADPs from the X-ray experiment were on average only 1% larger than the corresponding ADPs from neutron data ($\langle U_{ii}(X)/U_{ii}(N)\rangle = 1.011(16)$) . The average difference of the principal components of U_{ij} is 0.00091(80) Å^2, and the root mean-square value of $\Delta U_{ii}/\sigma$ is 1.42. These are excellent values for such a large molecular structure. This good agreement gave confidence that the deconvolution of the thermal motion yields the static EDD that was used in further analysis. Furthermore it demonstrated that the neutron values for hydrogen positions and ADPs can be incorporated into X-ray refinement. It should be mentioned that the data strongly suggested that quadrupolar electron density functions on the hydrogen sites should be used. This has been observed previously,[52] but we note that many studies in the literature only employ dipolar functions in modeling of hydrogens.[11c] The quadrupolar functions were responsible for modeling the significant polarization of the charge density that was observed in the strong hydrogen bonds. The adequacy of the refined model was demonstrated in the low residual densities (see Figures S1 – S5 in the Supporting Information). The highest residual is below 0.15 e Å^{-3}.

The synchrotron and the tube X-ray data may be compared to validate the quality of the former technique. Table 6 lists residuals for the two sets of common reflections as refined by both an independent atom model (IAM) and by the full multipole model derived from the combined data set. In these refinements, only the scale factor was varied. The two common data subsets matched almost equally well the two models; which means that we have not biased the model towards either of the two datasets.

Table 6. Refinement residuals for common reflections of the independent atom model (IAM) and the multipole model (MM). The first line gives results for the tube data, the second line for the synchrotron data.

	*R*1	*R*2	*wR*1	*wR*2	*S*
IAM	0.044	0.066	0.049	0.097	2.4
	0.039	0.060	0.049	0.094	2.7
MM	0.019	0.028	0.021	0.042	1.0
	0.017	0.033	0.019	0.037	1.1

Acknowledgement

Work at Argonne is supported by the US Department of Energy, BES-Materials Science, under contract No. W-31-109-ENG-38. The SUNY X3 beam line at NSLS is supported by the Division of Basic Energy Sciences of the US Department of Energy (DE-FG02-86ER45231). The synchrotron work is supported by the DANSYNC grant from the Danish Research Councils. B.B.I. and B.S. acknowledge financial support from the Danish Research Councils. The work was supported in part by the National Science Foundation (grant CDA96 – 01954 by Silicon Graphics, Inc) and by the NCSA at the University of Illinois, Urbana-Champaign (grant MCB970001N). Dr. Carlo Gatti is thanked for fruitful discussions and for assistance in evaluating the source function.

[1] D. M. Blow, J. J. Birktoft, B. S. Hartley, *Nature* **1969**, *221*, 337 – 340.
[2] a) J. A. Gerlt, P. G. Gassman, *Biochemistry* **1993**, *32*, 11943 – 11952; b) P. A. Frey, S. A. Whitt, J. B. Tobin, *Science* **1994**, *264*, 1927 – 1930; c) J. B. Tobin, S. A. Whitt, C. S. Cassidy, P. A. Frey, *Biochemistry* **1995**, *34*, 6919 – 6924; d) W. W. Cleland, P. A. Frey, J. A. Gerlt, *J. Biol. Chem.* **1998**, *273*, 25529 – 25532; e) J. A. Gerlt, M. M. Kreevoy, W. W. Cleland, P. A. Frey, *Chem. Biol.* **1997**, *4*, 259 – 267; f) C. S. Cassidy, J. Lin, P. A. Frey, *Biochemistry* **1997**, *36*, 4576 – 4584; g) A. Kahyaoglu, K. Haghjoo, F. Guo, F. Jordan, C. Kettner, F. Felfoldi, L. Polgar, *J. Biol. Chem.* **1997**, *272*, 25547 – 25554; h) C. S. Kraik, S. Roczniak, C. Largman, W. J. Rutter, *Science* **1987**, *237*, 909 – 913; i) W. R. Cannon, S. R. Benkovic, *J. Biol. Chem.* **1998**, *273*, 26527 – 26260; j) J. P. Guthrie, R. Kluger, *J. Am. Chem. Soc.* **1993**, *115*, 11569 – 11572; k) J. P. Guthrie, *Chem. Biol.* **1996**, *3*, 163 – 170; l) C. S. Cassidy, J. Lin, P. A. Frey, *Biochem. Biophys. Res. Commun.* **2000**, *273*, 789 – 792.
[3] F. Hibbert, J. Emsley, *Adv. Phys. Org. Chem.* **1990**, *26*, 255 – 379.
[4] a) A. Warshel, *J. Biol. Chem.* **1998**, *273*, 27035 – 27038; b) A. Warshel, A. Papazyan, P. A. Kollman, W. W. Cleland, M. M. Kreevoy, P. A. Frey, *Science* **1995**, *269*, 102 – 106; c) A. Warshel, A. Papazyan, *Proc. Natl. Acad. Sci. USA* **1996**, *93*, 13665 – 13670.
[5] C. L. Perrin, *Science* **1994**, *266*, 1665 – 1668.
[6] a) G. K. H. Madsen, B. B. Iversen, F. K. Larsen, M. Kapon. G. M. Reisner, F. H. Herbstein, *J. Am. Chem. Soc.* **1998**, *120*, 10040 – 10045; b) B. Schiøtt, B. B. Iversen, G. K. H. Madsen, F. K. Larsen, T. C. Bruice, *Proc. Natl. Acad. Sci. USA* **1998**, *95*, 12799 – 12802; c) B. Schiøtt, B. B. Iversen, G. K. H. Madsen, T. C. Bruice, *J. Am. Chem. Soc.* **1998**, *120*, 12117 – 12124; d) F. H. Herbstein, B. B. Iversen, M. Kapon, F. K. Larsen, G. K. H. Madsen, G. M. Reisner, *Acta Crystallogr. Sect. B* **1999**, *55*, 767 – 787.
[7] a) Y. Pan, M. A. McAllister, *J. Am. Chem. Soc.* **1997**, *119*, 7561 – 7566; b) Y. Pan, M. A. McAllister, *J. Am. Chem. Soc.* **1998**, *120*, 166 – 169; c) Y. Pan, M. A. McAllister, *J. Org. Chem.* **1997**, *62*, 8171 – 8176; d) C. J. Smallwood, M. A. McAllister, *J. Am. Chem. Soc.* **1997**, *119*, 11277 – 11281; e) G. A. Kumar, M. A. McAllister, *J. Am. Chem. Soc.* **1998**, *120*, 3159 – 3165.
[8] a) M. Garcia-Viloca, A. Gonzalez-Lafont, J. M. Lluch, *J. Am. Chem. Soc.* **1997**, *119*, 1081 – 1086; b) M. Garcia-Viloca, A. Gonzalez-Lafont, J. M. Lluch, *J. Phys. Chem.* **1997**, *101*, 3880 – 3886; c) J. Chen, M. A. McAllister, J. K. Lee, K. N. Houk, *J. Org. Chem.* **1998**, *63*, 4611 – 4619.
[9] S. Shan, S. Loh, D. Herschlag, *Science* **1996**, *272*, 97 – 101.
[10] G. A. Jeffrey, *An Introduction to Hydrogen Bonding*, Oxford University Press, New York, **1997**.
[11] a) E. Espinosa, C. Lecomte, E. Molins, *Chem. Phys. Lett.* **1999**, *300*, 745 – 748; b) E. Espinosa, C. Lecomte, E. Molins, *Chem. Phys. Lett.* **1998**, *285*, 170 – 173; c) E. Espinosa, M. Souhassou, H. Lachekar, C. Lecomte, *Acta Crystallogr. Sect. B* **1999**, *55*, 563 – 572.
[12] J. J. Danneberg, R. Rios, *J. Phys. Chem.* **1994**, *98*, 6714 – 6718.
[13] V. Barone, C. Adamo, *J. Chem. Phys.* **1996**, *105*, 11007 – 11019.
[14] T. Steiner, *J. Phys. Chem. A* **1998**, *102*, 7041 – 7052.
[15] P. Roversi, M. Barzaghi, F. Merati, R. Destro, *Can. J. Chem.* **1996**, *74*, 1145 – 1161.
[16] a) J. Overgaard, B. Schiøtt, F. K. Larsen, A. J. Schultz, J. C. MacDonald, B. B. Iversen, *Angew. Chem.* **1999**, *111*, 1321 – 1324; *Angew. Chem. Int. Ed.* **1999**, *38*, 1239 – 1242; b) G. K. H. Madsen, C. Wilson, T. M. Nymand, G. J. McIntyre, F. K. Larsen, *J. Phys. Chem.* **1999**, *103*, 8684 – 8690. c) P. Macchi, B. B. Iversen, A. Sironi, B. C. Chakoumakos, F. K. Larsen, *Angew. Chem.* **2000**, *112*, 2831 – 2834; *Angew. Chem. Int. Ed.* **2000**, *39*, 2719 – 2722.
[17] a) D. Madsen, C. Flensburg, S. Larsen, *J. Phys. Chem. A* **1998**, *102*, 2177 – 2188; b) C. Flensburg, S. Larsen, R. F. Stewart, *J. Phys. Chem.* **1995**, *99*, 10130 – 10141.
[18] For N–H···O interactions, Gilli and co-workers have recently presented comprehensive structural correlations for resonance-assisted hydrogen bonds: P. Gilli, V. Bertolasi, V. Ferretti, G. Gilli, *J. Am. Chem. Soc.* **2000**, *122*, 10405 – 10417.
[19] C. Gatti, R. F. W. Bader, *Chem. Phys. Lett.* **1998**, *287*, 233 – 238.
[20] T. Steiner, W. Saenger, *Acta Crystallogr. Sect. B* **1994**, *50*, 348 – 357.
[21] M. Würtele, M. Hahn, K. Hilpert, W. Höhne, *Acta Crystallogr. Sect. D* **2000**, *56*, 520 – 523.
[22] P. Kuhn, M. Knapp, S. M. Soltis, G. Ganshaw, M. Thoene, R. Bott, *Biochemistry* **1998**, *37*, 13446 – 13452.
[23] D. Neidhart, Y. Wei, C. Cassidy, J. Lin, W. W. Cleland, P. A. Frey, *Biochemistry* **2001**, *40*, 2439 – 2447.
[24] R. F. W. Bader, *Atoms in Molecules: A Quantum Theory*, Oxford University Press, Oxford, **1990**.
[25] Y. Abramov, *Acta Crystallogr. Sect. A* **1997**, *53*, 264 – 272.

  0947-6539/01/0717-3766 $ 17.50+.50/0

[26] F. W. Biegler-König, R. F. W. Bader, T. -H. Tang, *J. Comput. Chem.* **1982**, *3*, 317–328.
[27] a) M. Souhassou, C. Lecomte, R. H. Blessing, A. Aubry, M. M. Rohmer, R. Wiest, M. Benard, M. Marraud, *Acta Crystallogr. Sect. B* **1991**, *47*, 253–266; b) M. Souhassou, C. Lecomte, N. E. Ghermani, M. M. Rohmer, R. Wiest, M. Benard, R. H. Blessing, *J. Am. Chem. Soc.* **1992**, *114*, 2371–2382; c) V. Pishon-Pesme, C. Lecomte, H. Lachekar, *J. Phys. Chem.* **1995**, *99*, 6242–6250.
[28] a) G. S. Chandler, B. N. Figgis, P. A. Reynolds, S. K. Wolff, *Chem. Phys. Lett.* **1994**, *225*, 421–426. b) B. B. Iversen, F. K. Larsen, B. Figgis, P. A. Reynolds, *Trans. Am. Crystallogr. Assoc.* **1995**, *31*, 1–10.
[29] C. Gatti, personal communication.
[30] For more comprehensive NMR tables and structural correlations consult for example:a) P. Gilli, V. Bertolasi, V. Ferretti, G. Gilli, *J. Am. Chem. Soc.* **2000**, 122, 10405–10417. b) W. D. Arnold, E. Oldfield, *J. Am. Chem. Soc.* **2000**, 122, 12835–12841.
[31] NMR measurements thanks to Dr. J. Skibsted, Instrument Center for Solid-State NMR Spectroscopy, Department of Chemistry, University of Aarhus, Denmark.
[32] In transition metal bonding it is well known that coordination bonds may have very different covalent contributions, but this is not an indication of the bond strength. See for example: a) G. Frenking, U. Pidum, *J. Chem. Soc. Dalton. Trans.* **1997**, 1653–1662. b) P. E. M. Siegbahn, *J. Phys. Chem.* **1993**, *97*, 9096–9102. c) P. Macchi, A. J. Schultz, F. K. Larsen, B. B. Iversen, *J. Phys. Chem.* **2001**, in press.
[33] Several complexes between formed chymotrypsin and TS-inducing substrates have been studied by using ^{1}H NMR spectroscopy. The following chemical shifts have been assigned to the His–Asp HB, analogous to HB2: δ_H (ppm): 16.5[29a], 17.2[29a], 18.7[29b], 18.6,[2f] 18.9[29a] and similar values.[23] The ^{1}H NMR spectrum of **1** shows a broad maximum at $\delta = 14.8$, which consists of the signals for all three short N–H···O HB's. Thus the environment around H3A in **1** is different from the corresponding hydrogen in the catalytic triad in its activated state. a) T. -C. Liang, R. H. Abeles, *Biochemistry* **1987**, *26*, 7603–7608; b) G. Robillard, R. G. Shulman, *J. Mol. Biol.* **1972**, *72*, 507–511.
[34] A. J. Schultz, K. Srinivasan, R. G. Teller, J. M. Williams, C. M. Lukehart, *J. Am. Chem. Soc.* **1984**, *106*, 999–1003.
[35] a) A. J. Schultz, P. C. W. Leung, *J. Phys Colloq.* **1986**, *5*, 137–142; b) A. J. Schultz, *Trans. Am. Crystallogr. Assoc.* **1987**, *23*, 61–69.
[36] M. Lehmann, F. K. Larsen, *Acta Crystallogr. Sect. A* **1974**, *30*, 580–584.
[37] V. F. Sears, *Neutron News* **1992**, *3*, 26–37.
[38] J. A. K. Howard, O. Johnson, A. J. Schultz, A. M. Stringer, *J. Appl. Crystallogr.* **1987**, *20*, 120–122.
[39] A. Darovsky, R. Bolotovsky, P. Coppens, *J. Appl. Crystallogr.* **1994**, *27*, 1039–1040.
[40] Z. Otwinowski, *Oscillation Data Reduction Program*, in *Data Collection and Processing*, Proceedings of the CCP4 Study Weekend, Jan 29–30, **1993**.
[41] R. Bolotovsky, M. White, A. Darovsky, P. Coppens, *J. Appl. Crystallogr.* **1995**, *28*, 86–95.
[42] J. Zalelski, G. Wu, P. Coppens, *J. Appl. Crystallogr*. **1998**, *31*, 302–304.
[43] R. H. Blessing, *J. Appl. Crystallogr.* **1989**, *22*, 396–397.
[44] P. Coppens, *Program DATAP*, Chemistry Department, state University of New York at Buffalo, Buffalo, New York 14260-3000, (USA).
[45] M. J. Frisch, G. W. Trucks, H. B. Schlegel, P. M. W. Gill, B. G. Johnson, M. A. Robb, J. R. Cheeseman, T. A Keith, G. A. Peterson, J. A. Montgomery, K. Raghavachari, M. A. Al-Laham, V. G. Zakrzewski, J. V. Ortiz, J. B. Foresman, J. Cioslowski, B. B. Stefanov, A. Nanayakkara, M. Challacombe, C. Y. Peng, P. Y. Ayala, W. Chen, M. W. Wong, J. L. Andres, E. S. Repogle, R. Gomperts, R. L. Martin, D. J. Fox, J. S. Binkley, D. J. Defrees, J. Baker, J. J. P. Stewart, M. Head-Gordon, C. Gonzalez, J. A. Pople, Gaussian 94, Revision B.2 Gaussian, Pittsburg, PA, **1995**.
[46] J. C. MacDonald, unpublished results.
[47] B. B. Iversen, F. K. Larsen, A. A. Pinkerton, A. Martin, A. Darovsky, P. A. Reynolds, *Acta Crystallogr. Sect. B* **1999**, *55*, 363–374.
[48] N. K. Hansen, P. Coppens, *Acta Crystallogr. Sect. A* **1978**, *34*, 909–921.
[49] T. Koritszansky, S. T. Howard, P. R. Mallinson, Z. Su, T. Richter, N. K. Hansen, *XD, a Computer Program Package for Multipole Refinement and Analysis of Charge Densities from X-ray Diffraction Data*, Freie Universität Berlin, **1999**.
[50] A. El Haouzi, N. K. Hansen, C. Le Hénaff, J. Protas, *Acta Crystallogr. Sect. A* **1996**, *52*, 291–301.
[51] B. B. Iversen, F. K. Larsen, B. N. Figgis, P. A. Reynolds, A. J. Schultz, *Acta Crystallogr. Sect. A* **1996**, *52*, 923–931.
[52] a) B. N. Figgis, B. B. Iversen, F. K. Larsen, P. A. Reynolds, *Acta Crystallogr. Sect B* **1993**, *49*, 794–806; b) B. B. Iversen, F. K. Larsen, B. N. Figgis, P. A. Reynolds, *J. Chem. Soc. Dalton Trans.* **1997**, 2227–2240.

Received: January 5, 2001 [F2987]